MITSUBISHI ELECTRIC RESEARCH LABORATORIES
https://www.merl.com

Local Eigenmotion Control for Near Rectilinear Halo Orbits

Elango, Purnanand; Di Cairano, Stefano; Kalabic, Uros; Weiss, Avishai

TR2022-060 June 11, 2022

Abstract

The upcoming deployment of the Lunar Orbital Platform-Gateway (LOP-G) on a Near Rectilinear Halo Orbit (NRHO) calls for reliable, low-cost strategies for station keeping and relative motion tailor-made for NRHO. This paper proposes a control approach which harnesses the eigenvectors of state transition matrices (STM) associated with a high-fidelity NRHO solution in the ephemeris model to design long-term station keeping and bounded relative motion. The proposed method effectively utilizes the natural motion of the spacecraft so that control actions are infrequent and fuel efficient. The performance of the proposed approach is demonstrated via simulations with a state estimator that uses simulated mea- surements from the Deep Space Network.

American Control Conference (ACC) 2022

Mitsubishi Electric Research Laboratories, Inc.
201 Broadway, Cambridge, Massachusetts 02139

Local Eigenmotion Control for Near Rectilinear Halo Orbits

Purnanand Elango[1], Stefano Di Cairano[2], Uroš Kalabić[3], Avishai Weiss[4]

***Abstract*— The upcoming deployment of the Lunar Orbital Platform-Gateway (LOP-G) on a Near Rectilinear Halo Orbit (NRHO) calls for reliable, low-cost strategies for station keeping and relative motion tailor-made for NRHO. This paper proposes a control approach which harnesses the eigenvectors of state transition matrices (STM) associated with a high-fidelity NRHO solution in the ephemeris model to design long-term station keeping and bounded relative motion. The proposed method effectively utilizes the natural motion of the spacecraft so that control actions are infrequent and fuel efficient. The performance of the proposed approach is demonstrated via simulations with a state estimator that uses simulated measurements from the Deep Space Network.**

I. Introduction

The Lunar Orbital Platform-Gateway (LOP-G), also referred to as the Gateway, will play an important role in facilitating missions in cis-lunar space and beyond [1], [2]. The Gateway will be deployed in proximity to a near rectilinear halo orbit (NRHO), a closed periodic trajectory in the Earth-Moon circular-restricted three-body problem (CR3BP), due to its favourable stability properties and visibility from Earth [3].

The Gateway will be deployed *near* and not *on* an NRHO, because the NRHO of the CR3BP does not take into account perturbations such as the gravitational attraction of the Sun, solar radiation pressure (SRP), or lunar J2 effects. Instead of attempting to follow the NRHO of the CR3BP and using fuel to compensate for predictable perturbations, standard practice is to solve via multiple shooting or collocation-based techniques for a high-fidelity trajectory near an NRHO that accounts for all major predictable forces in cis-lunar space [4], [5]. This high-fidelity solution is also referred to as an NRHO, even though it is no longer closed, periodic, nor stable. The benefit of this high-fidelity NRHO solution, however, is that in the absence of any additional perturbing forces, a spacecraft could naturally follow the trajectory without expending any fuel, which is a key performance metric to ensure the long term viability of the Gateway.

In recent years, several station-keeping strategies have been developed for high-fidelity NRHOs, including target point methods [6]–[8], crossing control [9]–[11], Hamiltonian structure preserving strategy [8], [12] and Floquet mode control [6], [8], [13]. While the Gateway itself could make use of such control strategies, these methods can not be directly applied to visiting spacecraft such as cargo resupply, human transport, or inspection and maintenance missions, which may need to perform long-term bounded, collision-free relative motion about the Gateway. Given this need, we propose local eigenmotion-based control: a strategy for reliable, fuel-efficient station keeping and bounded relative motion control for the Gateway and its visiting spacecraft. While formation control for multiple spacecraft on halo orbits has been developed [14]–[16], for NRHO in particular, these methods propose control schemes based on the periodic solution in the CR3BP [17] and rely on the computationally expensive process of generating a high-fidelity solution for each spacecraft in the formation [18], [19]. The approach proposed in this work makes use of a single precomputed high-fidelity NRHO solution while ensuring safe separation distance between spacecraft.

While a nonlinear optimal control problem could be solved to obtain the optimal station-keeping maneuver for the entire duration of the spacecraft mission, such an approach is computationally prohibitive. The local eigenmotion-based control, on the other hand, exploits natural motion to provide a tractable method for fuel-efficient maneuvering, while also reducing the frequency of control action, which is another key performance metric for the long term viability of the Gateway due to thruster lifecycle. In contrast, LQR-based station keeping requires frequent control action, and re-planning a new trajectory in the high-fidelity model using multiple shooting or collocation whenever the spacecraft diverges away is prohibitively expensive for on-board computation.

Following the notation in this section, the paper proceeds in Section II with a description of NRHOs and the dynamical system model. Section III introduces the notion of local eigenmotion and develops the control algorithm. Section IV demonstrates the approach via a case study of two spacecraft in bounded relative motion about a high-fidelity NRHO that take simulated measurements from the Deep Space Network. Finally, concluding remarks are provided in Section V.

A. Notation

The set of natural numbers is $\mathbb{N}$ and the set of real numbers is $\mathbb{R}$. All vectors are column vectors. A real vector of length $n \in \mathbb{N}$ belongs to the set represented by $\mathbb{R}^n$. Vectors are represented as comma separated list of elements enclosed in $[\cdot]$. A vector with two elements $[a, b]$ with real numbers a and b such that $a \leq b$ also represents a closed interval on the real line. Similarly, (a, b) denotes an open interval. A vector constructed by vertically stacking two vectors c and d can be compactly represented as $[c^\top\ d^\top]^\top$. The vector of length

[1] P. Elango is with the William E. Boeing Department of Aeronautics and Astronautics University of Washington, Seattle, WA 98195. Email: pelango@uw.edu. He interned at MERL during the development of this work.

[2,3,4] S. Di Cairano, U. Kalabić, and A. Weiss are with Mitsubishi Electric Research Laboratories (MERL), Cambridge, MA 02139, USA. Emails: {dicairano,kalabic,weiss}@merl.com

n containing zeros is denoted by 0_n.

The kth element of a vector θ of length $n \geq k$ is denoted by $\theta[k]$. Given a matrix Θ with $n \geq k$ rows and $m \geq k$ columns, row k is denoted by $\Theta[k,:]$, while column k is denoted by $\Theta[:,k]$. If κ is a vector consisting of elements from $\{1,\ldots,n\}$, then $\theta[\kappa]$ is a vector of elements of θ indexed by the elements in the vector κ. Similarly, $\Theta[:,\kappa]$ and $\Theta[\kappa,:]$ are matrices composed of columns and rows of Θ, respectively, indexed by the elements in the vector κ.

The identity matrix is denoted by I, with its dimension inferred by context. An eigenvalue of a matrix is denoted by λ unless otherwise specified.

II. NRHO Model

Near rectilinear halo orbits (NRHO) are periodic trajectories around the L1 and L2 Lagrange points of the Earth-Moon circular restricted three-body problem (CR3BP). Owing to their favorable stability properties and relatively low station-keeping cost, the NRHO about the L2 point with 9:2 synodic resonance and perilune radius of about 3150 km has been chosen for deploying the Gateway [1], [20]. However, NRHOs don't exist in reality since the CR3BP ignores solar radiation pressure (SRP), gravitational forces due to celestial bodies other than Earth and Moon, and effects like lunar J2 zonal harmonics. Ignoring these higher order effects during mission design would lead to an unacceptably high amount of fuel consumption. Thus, a high-fidelity astrodynamics model with ephemeris data is used in practice to generate a solution which is closest to the NRHO in the CR3BP. This high-fidelity solution is aperiodic and consists of a finite number of revolutions around the Moon. The astrodynamics model considered in this work is based on the one used in [21], which accounts for all major predictable forces acting on a spacecraft in cis-lunar space. Any major predictable force has magnitude larger than that of the largest unpredictable force. For the model considered here, the largest unpredictable force influencing a spacecraft is determined to be the indirect disturbance caused by navigation error feeding into the spacecraft's controller [22]. The navigation error is quantified under the assumption that the spacecraft state is estimated using measurements from the Deep Space Network (DSN) [23], [24]. Under these assumptions, the force-magnitude analysis in [21] determined that the major predictable forces acting on a spacecraft in the region of space occupied by the NRHO of the CR3BP are SRP, lunar J2 zonal harmonics, and gravitational forces due to the Earth, Moon and Sun.

Let the high-fidelity dynamical system be represented by

$$\dot{\theta}(t) = g(t,\theta(t),u(t)), \tag{1}$$

which describes the equations of motion of a spacecraft in the non-inertial rotating frame (henceforth referred to as the rotating frame) considered in the CR3BP. The origin of this frame is at the Earth-Moon barycenter, with x-axis pointing towards the center of mass of Moon and z-axis along the angular momentum vector of the Earth-Moon system in the CR3BP. This frame is commonly chosen for the analysis of NRHOs since it is relevant for observation and communication from Earth [4, Section 2.1.2]. The right-hand-side of the model in (1) accounts for the major predictable external forces acting on the spacecraft mentioned above. Interested readers can refer to [25, Section 2.3] for further details. The state vector $\theta \triangleq [r^\top \; v^\top]^\top$ consists of the spacecraft position vector r and velocity vector v in the rotating frame, and u represents the control input vector.

A. Control Model

The control approach developed in the following section makes use of impulsive thrusters to execute maneuvers, wherein a thrust impulse is modelled to cause an instantaneous change in velocity of the spacecraft. Consider the motion of the spacecraft in the time interval $[t_1,t_2]$ with a thrust impulse $\zeta \in \mathbb{R}^3$ applied at $t' \in (t_1,t_2)$. The control input $u(t)$ can be represented as

$$u(t) = \begin{bmatrix} 0_3 \\ \zeta \end{bmatrix} \delta(t-t'), \quad \text{for } t \in [t_1,t_2], \tag{2}$$

where $\delta(t)$ is the Dirac delta function. The right-hand-side of (1) can be rewritten as

$$g(t,\theta(t),u(t)) = f(t,\theta(t)) + u(t), \tag{3}$$

for $t \in [t_1,t_2]$, where f includes the previously mentioned external forces acting on the spacecraft. The (uncontrolled) natural motion of the spacecraft is thus given by

$$\dot{\theta}(t) = f(t,\theta(t)). \tag{4}$$

The spacecraft state at t_2 obtained after the impulse at t' can be then determined as follows

$$\begin{aligned} \theta(t_2) &= \theta(t_1) + \int_{t_1}^{t_2} g(\tau,\theta(\tau),u(\tau))\mathrm{d}\tau, \\ &= \theta(t_1) + \int_{t_1}^{t_2} \left(\begin{bmatrix} 0_3 \\ \zeta \end{bmatrix} \delta(\tau-t') + f(\tau,\theta(\tau)) \right) \mathrm{d}\tau, \\ &= \theta(t') + \int_{t'}^{t_2} f(\tau,\theta(\tau))\mathrm{d}\tau, \end{aligned} \tag{5}$$

where

$$\theta(t') = \theta(t_1) + \begin{bmatrix} 0_3 \\ \zeta \end{bmatrix} + \int_{t_1}^{t'} f(\tau,\theta(\tau))\mathrm{d}\tau. \tag{6}$$

While the propagation of spacecraft dynamics with impulsive thrust (6) is used in the subsequent development, with minor modifications, the control approach of Section III can be adapted for thrust pulses of finite-duration. Note that finite-duration thrust pulses on the order of minutes can be approximated fairly well by thrust impulses due to the sufficiently slow time scales of the system dynamics (4).

B. Baseline Solution and Linearization

Denote the high-fidelity NRHO solution of (4) as the baseline solution $\bar{\theta}(t)$. The baseline solution is an uncontrolled, natural motion trajectory which lies near the NRHO of the CR3BP, and is estimated using the multiple shooting approach in [4]. The baseline solution $\bar{\theta}(t)$ consists of $K \triangleq 60$ revolutions around the Moon spanning $t_{\max} \triangleq 394$

days, where $t \in [0, t_{\max}]$ with $t = 0$ corresponding to the Julian date epoch of January 13, 2023. The position in each revolution which is farthest from the moon is referred to as an apolune, and the corresponding time instants are of particular importance to the control strategy of Section III. Apolune approach times for K revolutions of $\bar{\theta}(t)$ are given by $t^0_{\text{apo}} < t^1_{\text{apo}} < \ldots < t^K_{\text{apo}}$, where $t^0_{\text{apo}} = 0$ and $t^K_{\text{apo}} = t_{\max}$.

In addition to the baseline, the following section makes use of the linear time-varying system,

$$\dot{\theta}(t) \approx A(t)\theta(t) + b(t), \tag{7}$$

where,

$$A(t) = \left.\frac{\partial f(\tau, \omega)}{\partial \omega}\right|_{(t, \bar{\theta}(t))}, \tag{8a}$$

$$b(t) = (I - A(t))\bar{\theta}(t), \tag{8b}$$

which approximates solutions of (4) near $\bar{\theta}(t)$.

The proposed control strategy aims to keep the spacecraft in the region of the state space close to the baseline[1] where the linear approximation (7), which, along with $\bar{\theta}(t)$, can be computed a priori, is valid. Hence, the linear model, although imperfect, is useful for predicting future evolution of the nonlinear dynamics (4) and for determining appropriate control action.

The finite-time behavior of solutions to (4) near the baseline solution is particularly useful and can be analyzed using the discrete-time counterpart of (7). More precisely, if the spacecraft is at θ_1 in the vicinity of $\bar{\theta}(t_1)$ for some $t_1 \in [0, t_{\max}]$, then its state at $t_2 > t_1$, denoted by θ_2, can be approximated as

$$\theta_2 \approx \Phi(t_2, t_1)\theta_1 + \chi(t_2, t_1), \tag{9}$$

where $\Phi(t_2, t_1)$ is the state transition matrix (STM) for the time interval $[t_1, t_2]$ obtained by propagating the linear system

$$\dot{\Phi}(t, t_1) = A(t)\Phi(t, t_1), \quad t \geq t_1, \tag{10}$$

over the time interval $[t_1, t_2]$ with initial condition $\Phi(t_1, t_1) = I$, and $\chi(t_2, t_1)$ is the residual

$$\chi(t_2, t_1) = \int_{t_1}^{t_2} \Phi(t_2, \tau) b(\tau) \mathrm{d}\tau. \tag{11}$$

For an eigenvector ν of $\Phi(t_2, t_1)$, there exists a complex number λ such that

$$\Phi(t_2, t_1)\nu = \lambda\nu. \tag{12}$$

If $|\lambda| \leq 1$ then ν is said to be a *non-expanding* eigenvector, whereas if $|\lambda| > 1$ then ν is said to be an *expanding* eigenvector. The STM provides useful local information about the solutions to (4) near $\bar{\theta}(t)$. The natural motion that results from an initial condition along the expanding and non-expanding eigenvectors of an STM is termed as *expanding* and *non-expanding local eigenmotion*, respectively. Ideally, a non-expanding local eigenmotion associated with $\Phi(t_2, t_1)$ does not diverge away from the baseline for the time interval $[t_1, t_2]$, whereas an expanding local eigenmotion diverges away during the same interval. In practice, a non-expanding local eigenmotion can still diverge away for $t < t_2$ owing to the fact that the linear estimate in (9) is only an approximation of the propagated nonlinear dynamics (4). Since the linear model is only valid close to the baseline, the performance of a non-expanding local eigenmotion can deteriorate when the initial condition is far away from $\bar{\theta}(t)$.

[1]The region where deviation of the spacecraft from the baseline is much smaller than the scale of the baseline.

III. Local Eigenmotion Control

The proposed control approach utilizes STMs computed for a sequence of adjacent time intervals spanning $[0, t_{\max}]$, termed as *receding-horizon* STMs, to determine non-expanding local eigenmotion corresponding to those intervals. Whenever the spacecraft is predicted to diverge beyond a specified threshold from the baseline $\bar{\theta}(t)$, it is maneuvered to an initial condition of one of the non-expanding local eigenmotions in a fuel-efficient manner. In principle, we could compute an STM for the entire duration of the baseline, and pick a non-expanding eigenmotion to obtain a bounded relative motion trajectory for the entire duration of the baseline in one shot. However, this approach is computationally infeasible because the condition number of the STM increases as the time duration for which it holds increases. In practice, the longest time duration for which the STM is reliable is typically the time required for 12 revolutions around the Moon, which is about 78 days.

The strategy developed in this work considers maneuvers at apolune [21], but not necessarily every time the spacecraft visits apolune. The reason for this is as follows. For some $G \leq 12$ and $k \leq K - G$, assume that the spacecraft is initialized on a desirable local eigenmotion in proximity to the baseline by precisely placing it on an appropriate eigenvector of $\Phi(t^{k+G}_{\text{apo}}, t^k_{\text{apo}})$. Numerical simulations of (4) indicate that the spacecraft exhibits satisfactory bounded motion relative to the baseline for at least the following G revolutions around the Moon.

As previously mentioned, the longest time duration for which the STM is numerically reliable, which here means a condition number smaller then 10^8, is the time required for $H \triangleq 12$ revolutions around the Moon. The eigenvalues of the STM estimated for $[t^0_{\text{apo}}, t^H_{\text{apo}}]$ are $\text{spec}(\Phi(t^H_{\text{apo}}, t^0_{\text{apo}})) = \{1.14 \times 10^4,\ 4.48,\ -0.88 + \text{i}0.46,\ -0.88 - \text{i}0.46,\ 0.22,\ 8.75 \times 10^{-5}\}$. Observe that this STM has two expanding and four non-expanding eigenvectors. Owing to a significantly large eigenvalue, small perturbations to a spacecraft on the baseline NRHO solution can cause it to diverge away rapidly. This is in stark contrast to the favorable stability properties of the NRHO in CR3BP model. Furthermore, it is observed that the spectrum of the STM estimated for $[t^k_{\text{apo}}, t^{k+H}_{\text{apo}}]$ for any $k \leq K - H$ is qualitatively similar that of the first H revolutions. As a result, typically any vector in the span of the four non-expanding eigenvectors of $\Phi(t^{k+H}_{\text{apo}}, t^k_{\text{apo}})$ give rise to a non-expanding local eigenmotion for any $k \leq K - H$. Let these

eigenvectors, indexed by the set $\mathcal{I}^k$, be denoted by ν_i^k for $i \in \mathcal{I}^k,\ k \leq K-H$.

The spacecraft maneuvers occur over a short time interval, referred to as the control horizon, just before the spacecraft reaches an apolune. A maneuver to return the spacecraft state to a non-expanding local eigenmotion is initiated when a trigger condition is met. Let the position deviation of the spacecraft at $t = t_{\text{apo}}^k$ be denoted by Δr_k for $k \leq K-H$. The trigger condition adopted in this work considers the change in distance between the spacecraft and the baseline solution since $t = 0$ and since its recent visit to apolune, and is given by

$$\Delta r_k > \min\left\{\rho \Delta r_0, \min\{2\Delta r_{k-1}, \Delta r_0\}\right\}, \tag{13}$$

where, ρ is a tuning parameter that contributes to determining the nature of the generated bounded motion trajectory near the baseline.

If the trigger condition (13) is satisfied by Δr_k for some $k < K$, a fuel-efficient maneuver for transferring the spacecraft to a non-expanding local eigenmotion starting at t_{apo}^k is computed by solving the discrete-time optimal control problem

$$\underset{\substack{\{\alpha_i\}_{i\in\mathcal{I}},\\ \{u_j\}_{j=0}^{N-2}}}{\text{minimize}} \quad \sum_{j=0}^{N-2} \|u_j\|_2 \tag{14a}$$

$$\text{subject to} \quad \theta(\tau_{j+1}^k) = \theta(\tau_j^k) + \begin{bmatrix} 0_3 \\ u_j \end{bmatrix} + \int_{\tau_j^k}^{\tau_{j+1}^k} f(\gamma, \theta(\gamma))\mathrm{d}\gamma, \tag{14b}$$

$$0 \leq j \leq N-1,$$

$$\theta(\tau_{N-1}^k) = \bar{\theta}(\tau_{N-1}^k) + \sum_{i\in\mathcal{I}^k} \alpha_i \nu_i^k, \tag{14c}$$

$$\theta(\tau_0^k) = \hat{\theta}(\tau_0^k), \tag{14d}$$

for the time grid $T_N^k \triangleq [\tau_0^k, \ldots, \tau_{N-1}^k]$, where $\tau_j^k \triangleq t_{\text{apo}}^k - (N-1-j)\Delta t$ for $j = 0, \ldots, N-1$. The maneuver consists of $N-1$ thrust impulses $\{u_j\}_{j=0}^{N-2}$ applied at intervals of Δt starting from τ_0^k. Under the assumption of impulsive input, the representation of the propagated equations of motion in (6) is utilized for constraint (14b). The boundary condition (14c) stipulates that the state at end of the control horizon lies in the span of the non-expanding eigenvectors of $\Phi(t_{\text{apo}}^{k+H+1}, t_{\text{apo}}^{k+1})$, which would give rise to a non-expanding local eigenmotion. Furthermore, in a practical implementation, the controller will not have access to the true state of the spacecraft. It receives an estimate, denoted by $\hat{\theta}(\tau_0^k)$ in (14d), by the state estimator.

The proposed control approach results in the automatic routine summarized by Algorithm 1. The key components are described below.

- The input to Algorithm 1 consists of the following
  - The baseline solution $\bar{\theta}(t)$.
  - The time instants t_{apo}^k for $k = 0, \ldots, K$, corresponding to $K+1$ visits to apolune in the baseline.
  - The initial distance Δr_0 of the spacecraft from the baseline.
  - Number of downstream revolutions H for which the STM is computed.
  - The time intervals before each visit to apolune in the baseline solution (excluding the first), T_N^k for $k = 1, \ldots, K$, each with N grid points uniformly spaced by Δt.
- `Propagate`(ψ, T) returns the state after propagating the high-fidelity prediction model (4) with initial condition ψ for the time interval specified by the two-element vector T. When Algorithm 1 operates alongside a state-estimator, as demonstrated in Section IV, the first argument of `Propagate`, ψ, is an estimate of the spacecraft's current state.
- `PosDev`(θ, ψ) returns the position deviation between states θ and ψ.
- `EigenMotion`$(\Delta r, k, H)$ returns the state with a position deviation of Δr from the state at the kth apolune of the baseline, and lying along the vector $\sum_{i\in\mathcal{I}^k} \nu_i$, where ν_i for $i \in \mathcal{I}^k$ are the non-expanding eigenvectors of $\Phi(t_{\text{apo}}^{k+H}, t_{\text{apo}}^k)$.

Algorithm 1 Local Eigenmotion Control

Input: $\bar{\theta}(t), \{t_{\text{apo}}^j\}_{j=0}^K, \Delta r_0, H, \{T_N^j\}_{j=1}^K$

$T_H^0 \leftarrow [t_{\text{apo}}^0, t_{\text{apo}}^H]$
$t_0 \leftarrow t_{\text{apo}}^0$
$\theta \leftarrow$ `EigenMotion`$(\Delta r_0, 0, H)$
$\Delta v \leftarrow 0$
$(l, k) \leftarrow (1, 0)$
while $k \leq K-1-H$ **do**
  $\bar{\psi} \leftarrow \bar{\theta}(t_{\text{apo}}^{k+1})$
  $T \leftarrow [t_{\text{apo}}^k, T_N^{k+1}[1]]$
  $\widetilde{\theta} \leftarrow$ `Propagate`(θ, T)
  $T \leftarrow T_N^{k+1}[[1, N]]$
  $\theta \leftarrow$ `Propagate`$(\widetilde{\theta}, T)$
  $\Delta r_{k+1} \leftarrow$ `PosDev`$(\theta, \bar{\psi})$
  if `Trigger`$(\Delta r_{k+1}, \Delta r_k, \Delta r_0)$ **then**
    $T_H^{k+1} \leftarrow [t_{\text{apo}}^{k+1}, t_{\text{apo}}^{k+H+1}]$
    $(U_l, \Delta v_l) \leftarrow$ `OptCtrl`$(\widetilde{\theta}, \Delta r_{k+1}, T_N^{k+1}, T_H^{k+1})$
    $\theta \leftarrow$ `PropagateCtrl`$(\widetilde{\theta}, U_l, T_N^{k+1})$
    $(\Delta v, \Delta r_{k+1}) \leftarrow (\Delta v + \Delta v_l,$ `PosDev`$(\theta, \bar{\psi}))$
    $l \leftarrow l + 1$
  end if
  $k \leftarrow k + 1$
end while
$M \leftarrow l - 1$

Output: $\Delta v, \{U_j, \Delta v_j\}_{j=1}^M$

- `Trigger` evaluates to true if the trigger condition (13) is satisfied.
- `OptCtrl`$(\psi, \Delta r, T_N^k, T_H^k)$ solves the discrete-time optimal control problem (14) for the time interval T_N^k, i.e., for a maneuver to take place right before the spacecraft's kth apolune visit. Constraint (14c) is constructed using the non-expanding eigenvectors of the STM for the interval $T_H^k = [t_{\text{apo}}^k, t_{\text{apo}}^{k+H}]$, and the initial condition (14d) is specified by ψ. `OptCtrl` returns the control effort required for the maneuver, and the control solution estimated as a matrix with the control input for each τ_j^k for $j = 0, \ldots, N-2$ stacked row-wise.
- `PropagateCtrl`(ψ, U, T_N^k) propagates (1) over the control horizon T_N^k using the control solution U returned by `OptCtrl` with initial condition ψ.
- Δv_j for $j = 1, \ldots, M$ is the cost for M maneuvers initiated in Algorithm 1 over the duration $[0, t_{\max}]$. The cumulative cost of the M maneuvers is given by Δv.

IV. Results

This section demonstrates a practical implementation of the proposed control strategy by augmenting Algorithm 1 with a Kalman Filter which estimates states using simulated range and range-rate measurements from the Deep Space Network (DSN). The measurements are received at a rate of 6 hr which is reasonable for the DSN, and adequate for accurate state estimation. The errors in range and range-rate measurements come from standard normal distributions with standard deviation of 10 m and 1 mm s^{-1}, respectively. More details on the DSN error statistics can be found in [21].

The simulations were implemented in MATLAB ver. 2019b running on a MacBook Pro with 16 GB RAM and 2.6 GHz Intel 6-Core i7 processor. The proposed approach is demonstrated for the case of two spacecraft executing bounded relative motion in the vicinity of the baseline solution. In particular, the Gateway is subjected to tight station keeping about the baseline while a visiting spacecraft is made to execute collision-free relative motion near the Gateway.

The trajectory computed for the Gateway, referred to as Solution 1, uses $\rho = 10$, $\Delta t = 6$ hr, $\Delta r_0 = 0.5$ km, and $N = 4$, whereas the trajectory for the visiting spacecraft, referred to as Solution 2, is computed with $\rho = 2$, $\Delta t = 12$ hr, $\Delta r_0 = 50$ km, and $N = 6$. Certain parameters in Algorithm 1 influence the nature of the bounded motion solution. In particular, the choice of ρ in (13) and Δr_0 for the two Solutions are instrumental in ensuring that they remain collision-free. These parameters are tuned such that the resulting solutions are infrequent and fuel efficient.

It is worthwhile to note that the effect of navigation uncertainty is more prominent for tight station-keeping maneuvers near the baseline. When a maneuver is initiated close to the baseline, the final state (which lies close to the baseline and is aligned with the desired eigenvector) is more easily corrupted by navigation uncertainly owing to its small magnitude measured relative to the baseline. As a consequence, the spacecraft could be maneuvered to a state which is not properly aligned with the desired eigenvector, which will then cause the spacecraft to diverge prematurely. Hence, tight station keeping could potentially necessitate more annual maneuvers. This pitfall is avoided while generating Solution 1 by choosing a small value of Δr_0 and a large value for ρ. This allows the spacecraft to slowly offset from the baseline over a duration of 150 days and settle at a distance of about 9 km from the baseline where maneuvers are not triggered too often.

TABLE I: Annual station-keeping performance

	Solution 1	Solution 2
Maneuvers	13	15
Control duty cycle [% time annually]	0.8	2.05
Fuel consumption [m s^{-1}]	0.05	0.7

The annual station-keeping performance of Solutions 1 and 2 are shown in Table I, and the distance of the Solutions from the baseline as a function of time is shown in Fig. 1. With the proposed strategy, the annual station-keeping cost for the Gateway is comparable to that of state-of-the art techniques for station keeping on NRHO [21], [26]. The fuel required for the visiting spacecraft is significantly higher since it maintains a larger distance from the baseline than the Gateway. As such, each maneuver for transferring to a non-expanding local eigenmotion of the baseline is more expensive. Although the annual cost for Solution 2 is significantly higher than that for Solution 1, it is still comparable to the cost reported by competing techniques [21].

Another notable benefit of the proposed approach is the relatively few maneuvers required to sustain annual bounded motion. The black segments on Solutions 1 and 2 in Fig. 1 highlight the significantly small annual control duty cycle. Furthermore, Solutions 1 and 2 do not pose a risk of collision between the Gateway and the visiting spacecraft. The distance between the solutions is never smaller than 8 km, as shown in Fig. 2.

V. Conclusions

This work proposes a control strategy for bounded motion in the vicinity of a near rectilinear halo orbit (NRHO) where the Gateway will be deployed. The key idea is to initiate fuel-efficient thruster firing to transfer the spacecraft to a state which yields bounded natural motion for a finite time whenever the spacecraft diverges significantly away from the baseline solution. The effectiveness of the strategy is demonstrated via a realistic simulation which includes a state estimator taking simulated measurements from the Deep Space Network. The annual station-keeping performance in terms of total fuel consumption and the total maneuver duration is shown to be at par or better than competing state-of-the art techniques.

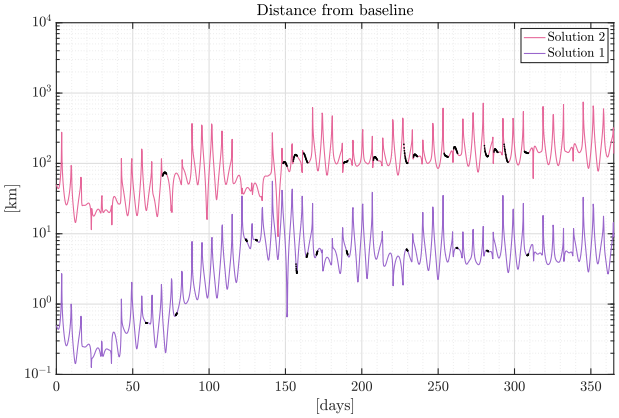

Fig. 1: Position deviations of Solution 1 (for Gateway) and Solution 2 (for the visiting spacecraft) with respect to the baseline are shown. The 13 maneuver segments of Solution 1 and 15 maneuver segments of Solution 2 are marked in black in black. The solutions seem to intersect at around 150 days, but that is only due to the log scale of the plot. Fig. 2 confirms that the least separation between the two solutions is at least 8 km.

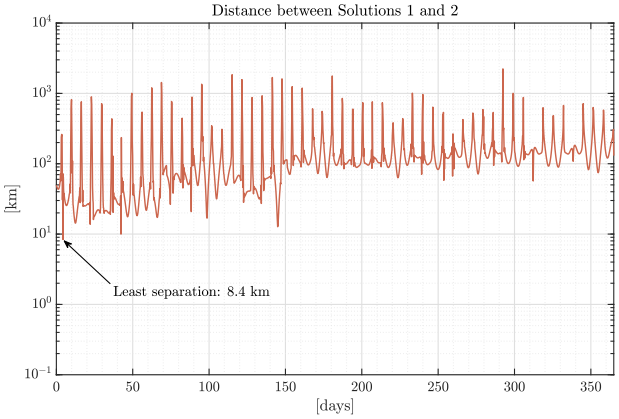

Fig. 2: Position deviation of Solution 1 (for Gateway) with respect to Solution 2 (for the visiting spacecraft) is shown. The two Solutions maintain a separation distance of at least 8 km at all times.

REFERENCES

[1] K. C. Laurini, B. Hufenbach, J. Hill, and A. Ouellet, "The global exploration roadmap and expanding human/robotic exploration mission collaboration opportunities," in *IAF 66th International Astronautical Congress*, October 2015, pp. 1–9.

[2] B. Hufenbach, K. Laurini, N. Satoh, C. Lange, R. Martinez, J. Hill, M. Landgraf, and A. Bergamasco, "International missions to lunar vicinity and surface - near-term mission scenario of the global space exploration roadmap," in *IAF 66th International Astronautical Congress*, October 2015, pp. 1–11.

[3] D. Lee, "Gateway destination orbit model: A continuous 15 year NRHO reference trajectory," NASA Johnson Space Center, Tech. Rep., 2019.

[4] T. A. Pavlak, "Trajectory design and orbit maintenance strategies in multi-body dynamical regimes," Ph.D. dissertation, Purdue University, 2013.

[5] Z. P. Olikara and D. J. Scheeres, "Numerical method for computing quasi-periodic orbits and their stability in the restricted three-body problem," *Advances in the Astronautical Sciences*, vol. 145, no. 911-930, 2012.

[6] K. C. Howell and T. M. Keeter, "Station-keeping strategies for libration point orbits-target point and Floquet mode approaches," *Spaceflight mechanics 1995*, pp. 1377–1396, 1995.

[7] G. Gómez, K. Howell, J. Masdemont, and C. Simó, "Station-keeping strategies for translunar libration point orbits," *Advances in Astronautical Sciences*, vol. 99, no. 2, pp. 949–967, 1998.

[8] S. Soldini, C. Colombo, and S. Walker, "Comparison of Hamiltonian structure-preserving and Floquét mode station-keeping for libration-point orbits," in *AIAA/AAS astrodynamics specialist conference*, 2014, p. 4118.

[9] D. Folta, T. Pavlak, K. Howell, M. Woodard, and D. Woodfork, "Stationkeeping of lissajous trajectories in the Earth-Moon system with applications to ARTEMIS," in *AAS/AIAA Space Flight Mechanics Meeting*, 2010.

[10] D. Rohrbaugh and C. Schiff, "Station-keeping approach for the microwave anisotropy probe (map)," in *AIAA/AAS Astrodynamics Specialist Conference and Exhibit*, 2002, p. 4429.

[11] D. J. Dichmann, C. M. Alberding, and W. H. Yu, "Stationkeeping monte carlo simulation for the James Webb Space Telescope," in *Proceedings 24th International Symposium on Space Flight Dynamics–24 th ISSFD, Laurel, MD, USA*, 2014.

[12] K. Tajdaran, "Incorporation of mission design constraints in Floquet mode and Hamiltonian structure-preserving orbital maintenance strategies for libration point orbits," Ph.D. dissertation, Purdue University, 2015.

[13] G. Gómez, J. Llibre, R. Martınez, and C. Simó, "Station keeping of a quasiperiodic halo orbit using invariant manifolds," in *Proceed. 2nd Internat. Symp. on spacecraft flight dynamics, Darmstadt*, 1986, pp. 65–70.

[14] B. Marchand and K. Howell, "Control strategies for formation flight in the vicinity of the libration points," *Journal of guidance, control, and dynamics*, vol. 28, no. 6, pp. 1210–1219, 2005.

[15] M. Bando and A. Ichikawa, "Formation flying along halo orbit of circular-restricted three-body problem," *Journal of Guidance, Control, and Dynamics*, vol. 38, no. 1, pp. 123–129, 2015.

[16] W. Wang, G. Mengali, A. A. Quarta, and J. Yuan, "Distributed adaptive synchronization for multiple spacecraft formation flying around Lagrange point orbits," *Aerospace Science and Technology*, vol. 74, pp. 93–103, 2018.

[17] S. Jung and Y. Kim, "Formation flying along unstable libration point orbits using switching Hamiltonian structure-preserving control," *Acta Astronautica*, vol. 158, pp. 1–11, 2019.

[18] B. T. Barden and K. C. Howell, "Fundamental motions near collinear libration points and their transitions," *The Journal of the Astronautical Sciences*, vol. 46, no. 4, pp. 361–378, 1998.

[19] K. C. Howell and B. G. Marchand, "Natural and non-natural spacecraft formations near the L1 and L2 libration points in the Sun–Earth/Moon ephemeris system," *Dynamical Systems*, vol. 20, no. 1, pp. 149–173, 2005.

[20] M. Duggan, X. Simon, and T. Moseman, "Lander and cislunar gateway architecture concepts for lunar exploration," in *2019 IEEE Aerospace Conference*. IEEE, 2019, pp. 1–9.

[21] V. Muralidharan, A. Weiss, and U. V. Kalabic, "Control strategy for long-term station-keeping on near-rectilinear halo orbits," in *AIAA Scitech 2020 Forum*, 2020. [Online]. Available: https://arc.aiaa.org/doi/abs/10.2514/6.2020-1459

[22] D. Davis, S. Bhatt, K. Howell, J.-W. Jang, R. Whitley, F. Clark, D. Guzzetti, E. Zimovan, and G. Barton, "Orbit maintenance and navigation of human spacecraft at cislunar near rectilinear halo orbits," in *AAS/AIAA Space Flight Mechanics Meeting*, 2017, pp. 1–20.

[23] C. L. Thornton and J. S. Border, *Radiometric tracking techniques for deep-space navigation*. John Wiley & Sons, 2003.

[24] K. C. Howell and S. C. Gordon, "Orbit determination error analysis and a station-keeping strategy for Sun-Earth L1 libration point orbits," *Journal of the Astronautical Sciences*, vol. 42, no. 2, pp. 207–228, 1994.

[25] V. Muralidharan, "Stretching directions in cislunar space: Stationkeeping and an application to transfer trajectory design," Ph.D. dissertation, Purdue University, 2021.

[26] D. Guzzetti, E. M. Zimovan, K. C. Howell, and D. C. Davis, "Stationkeeping analysis for spacecraft in lunar near rectilinear halo orbits," in *27th AAS/AIAA Space Flight Mechanics Meeting*, 2017, pp. 1–20.